



Cite this: RSC Adv., 2020, 10, 32137

Using *Fomitopsis pinicola* for bioinspired synthesis of titanium dioxide and silver nanoparticles, targeting biomedical applications†

Suriya Rehman, ^{*a} Rabindran Jermy, ^{*b} Sarah Mousa Asiri, ^d Manzoor A. Shah, ^c Romana Farooq, ^b Vijaya Ravinayagam, ^e Mohammad Azam Ansari, ^a Zainab Alsalem, ^a Reem Al Jindan, ^f Zafar Reshi, ^b and Firdos Alam Khan ^g

The current study proposes a bio-directed approach for the formation of titanium oxide and silver nanoparticles (TiO_2 and Ag NPs), using a wild mushroom, *Fomitopsis pinicola*, identified by 18S ribosomal RNA gene sequencing (gene accession no. MK635350) and phenotypic examination. NP synthesis was confirmed by X-ray diffraction (XRD), Fourier transform infrared spectroscopy (FT-IR), diffuse reflectance UV-visible spectroscopy (DR-UV), and scanning and transmission electron microscopy (SEM/TEM). Furthermore, the impact of NPs on *Escherichia coli* and *Staphylococcus aureus* and a human colon cancer cell line (HCT) were evaluated by MIC/MBC and MTT assays, respectively, along with structural morphogenesis by different microscopy methods. The results obtained showed that TiO_2 and Ag NPs were found to be significantly active, however, slightly enhanced antibacterial and anticancer action was seen with Ag NPs (10–30 nm). Such NPs can be utilized to control and treat infectious diseases and colon cancer and therefore have potential in a range of biomedical applications.

Received 22nd March 2020
 Accepted 20th May 2020

DOI: 10.1039/d0ra02637a
 rsc.li/rsc-advances

1. Background

In recent times, nanotechnology using metal NPs has been an extensively studied field, and involves the transition of bulk material to nanoscale size, introducing a remarkable effect on the properties, from increased surface synergy to quantum restrictions.¹ Metal NPs like silver, gold, zinc, titanium etc. are broadly used in different fields, like agriculture, medicine,

biomedical, electronic and other industries.^{1–3} The widely used method for the synthesis of these NPs is mostly chemical, which involves the use of a number of chemicals that could be detrimental to the ecosystem and human health. In contrast, the green synthesis of NPs, using organic sources, like plants, bacteria and fungi, is evolving as an influential field of nanotechnology, due to their safe, eco-friendly and cost-effective properties.⁴ Although, the demand for the green synthesis of NPs has been growing, inadequacy in the information and sources of green methods is preventing competitive chemical synthesis.

Fungi are one of the biological sources, broadly known for bioremediation utility, owing to their capability of mineralizing, a vast array of harmful compounds, with the help of enzymes, secreted to the environment.⁵ Additionally, lower and higher fungi are reported as mediators for the formation of NPs, because they produce huge amount of biomass and are easy to handle.^{5–9} Macrofungi (mushrooms) are excessively loaded in proteins and have been known for their nutrient-rich content and immense medicinal value. Though, only few studies have evaluated the possible application of mushrooms to produce metallic NPs, for which the possible reason could be their seasonal existence, as well as the extreme place of growth. Polyporoids are widely distributed in different biotopes and have been studied as reducing agent for the synthesis of various NPs. During the extracellular synthesis of many NPs like Au, Ag, *Volvariella volvacea*, *Trametes* Fr., *Trametes versicolor*, *Ganoderma lucidum* and *Ganoderma applanatum*, *Pleurotus florida*

^aDepartment of Epidemic Disease Research, Institute for Research & Medical Consultations, (IRMC), Imam Abdulrahman Bin Faisal University, Dammam, 31441, Saudi Arabia. E-mail: surrehman@iau.edu.sa; suriyamir@gmail.com; Web: https://scholar.google.com/scholar?hl=en&as_sdt=0%2C5&q=suriya+rehman

^bDepartment of Nano-Medicine Research, Institute for Research & Medical Consultations, (IRMC), Imam Abdulrahman Bin Faisal University, Dammam, 31441, Saudi Arabia. E-mail: rjermy@iau.edu.sa

^cDepartment of Botany, University of Kashmir, Srinagar, J&K, India

^dDepartment of Biophysics, Institute for Research & Medical Consultations, (IRMC), Imam Abdulrahman Bin Faisal University, Dammam, 31441, Saudi Arabia

^eDeanship of Scientific Research, Department of Nano-Medicine Research, Institute for Research & Medical Consultations (IRMC), Imam Abdulrahman Bin Faisal University, P. O. Box 1982, 31441 Dammam, Saudi Arabia

^fDepartment of Microbiology, College of Medicine, Imam Abdulrahman Bin Faisal University, Dammam, 31441, Saudi Arabia

^gDepartment of Stem Cell Research, Institute for Research & Medical Consultations, (IRMC), Imam Abdulrahman Bin Faisal University, Dammam, 31441, Saudi Arabia

† Electronic supplementary information (ESI) available. See DOI: 10.1039/d0ra02637a

‡ Prof. Zafar Reshi was not contactable during the revision process and therefore has not seen the final version of the manuscript.



have been reported as reducing and capping agent.^{8,10-12} Park and Park isolated laccase enzyme from *F. pinicola*, a brown-rot fungus fills Basidiomycota, Agaricomycetes, Fomitopsidaceae, which is the characteristic indicating its eligibility for potential in biological synthesis of NPs.¹³

To the best of the knowledge of authors, the ability of *F. pinicola*, to synthesize metallic NPs has not yet been studied. In the present work, we examined the ability of the wild mushroom sp., *F. pinicola*, to synthesize TiO_2 and Ag NPs, without using any supplementary reducing agent. The antimicrobial and anti-cancer potential of synthesized NPs was determined against human pathogens, *E. coli*, *S. aureus* and HCT cell line, respectively.

2. Methods

2.1. Collection, phenotypic and genotypic studies of *F. pinicola*

For the collection of sporocarps, standard method was followed¹⁴ (details of sample collection are provided in ESI†). Photographs were taken by Nikon D5300 DSLR Camera with a zoom lens of 18–140 VR. Passport data and the micro-habitat characteristics of collected sample was written in the field book. Sample was properly labeled, given a voucher number and carried to a laboratory for detailed morphometric examination.

Collected specimens were identified by keen observation of structures like pileus, stipe, their shape, structure, gill attachment etc., using standard keys (e.g., Mycokey, Index fungorum etc.) field guides and manuals. The samples were dried and deposited at the herbarium of the Centre for Biodiversity and Taxonomy, University of Kashmir, J&K, India. Microscopic features and measurements were made from slides prepared and stained with lactophenol cotton blue, 2% KOH and Melzer's reagent. For spore examination, the spores were tapped off the razor blade onto a clean and a drop of KOH or Melzer's reagent was added. Observation and photographs were captured at

magnification between 40 \times to 100 \times , using a Nikon Eclipse 80i microscope and phase contrast illumination (Nikon, Tokyo).

2.2. DNA isolation and PCR

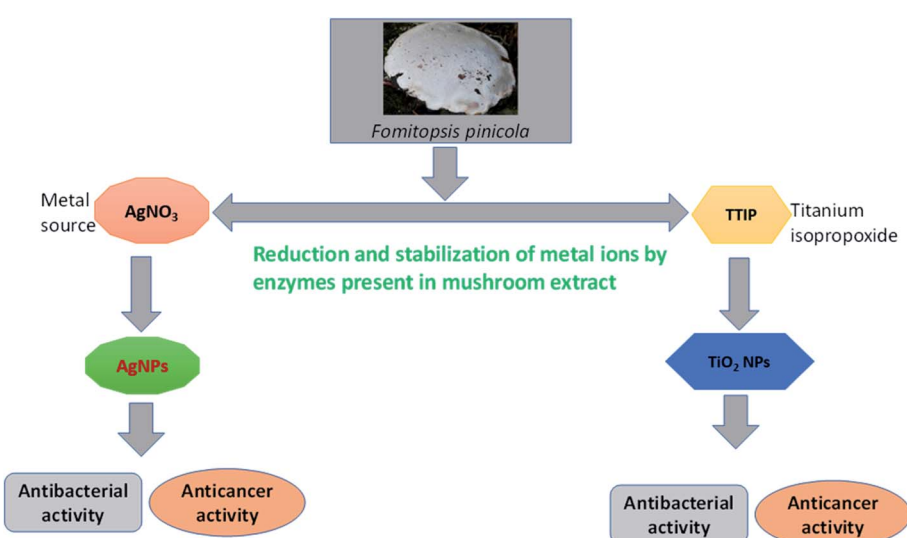
DNA extraction was done using manual CTAB method (cetyl trimethylammonium bromide).¹⁵ The extracted DNA was dissolved and preserved in TE (Tris-EDTA) buffer. The DNA was amplified for internal transcribed spacer (ITS) regions using the ITS1 and ITS4 in a PCR System Thermocycler Applied Biosystems with following parameters; denaturation for 10 min at 95 °C, 35 cycles at 95 °C for 1 min, 54 °C for 30 s and 72 °C for 2 min, followed by extension at 72 °C for 10 min. The purification of amplified products was done and sequenced with the same primers.¹⁵

2.3. Sequence and phylogeny analysis

The small subunit sequences were aligned with additional sequences downloaded from NCBI GenBank (<http://ncbi.nlm.nih.gov>) using BioEdit Sequence Alignment Editor (version 7.2.5).¹⁶ The sequence alignments and phylogenetic analysis were performed using MEGA 10 software (Tamura *et al.* 2011). Phylogeny was studied on ITS-18S rRNA genes in maximum likelihood method. Initial alignment was done using Clustal W software for maximum alignment and minimum gaps. The tree was generated by using the program DNADIST and NEIGHBOR from PHYLIP 3.69.¹⁷

2.4. Biosynthesis of TiO_2 and AgNPs using *F. pinicola*

The synthesis of TiO_2 and Ag NPs was conducted using the extract of *F. pinicola* by adopting a green synthesis method.¹¹ The samples were dried to obtain powder (10 g), which was further mixed with 100 mL of Millipore water and sonicated for 25–30 min. The sonicated mixture was centrifuged at the rpm of 4000 to obtain the clarified solution. Subsequently, the solution was filtered and stored at 4 °C. 10 mL of filtrate was mixed with



Scheme 1 Biosynthesis of TiO_2 and Ag NPs using the extract of *F. pinicola*.



1 mM AgNO_3 (100 mL) and put at room temperature on a shaker for agitation under observation, until the appearance of color change.¹¹ A similar procedure was followed for TiO_2 NPs, where 100 mL of 1 mM of titanium(IV) isopropoxide was used as source solution (Scheme 1). The mushroom extract to 1 mM AgNO_3 or $\text{Ti}(\text{OC}_3\text{H}_7)_4$ ratio used for the study was 1 : 10. Finally, the obtained NPs were filtered using Whatman filter paper, washed two times in ethanolic solution and centrifuged (4000 rpm) at 10 °C for 10 min. After drying, the sample was used for further studies.

2.5. Characterization of biosynthesized TiO_2 and AgNPs

The crystalline phase of TiO_2 and AgNPs was measured using benchtop X-ray diffractometer MiniFlex 600 (Rigaku, Japan). The coordination environment of TiO_2 and Ag NPs were analyzed using diffuse reflectance UV-visible spectroscopy (V-750, JASCO). The TiO_2 and AgNPs functional groups were analyzed using Fourier transform infrared spectroscopy (PerkinElmer). The surface morphology, distribution and features of TiO_2 and AgNPs were studied using SEM (Inspect S50) and TEM (Morgagni 268). For TEM analysis, samples were prepared by dispersing in ethanol followed by shaking in an ultrasonicator for 20 min, and then a suspended drop was dried at room temperature on the carbon-coated copper grid.¹⁸

2.6. Antibacterial activity of biosynthesized NPs

Antibacterial activity of synthesized, TiO_2 NPs and Ag NPs were studied against the human pathogenic Gram-negative bacteria and Gram positive bacteria, (*E. coli* ATCC35218 and *S. aureus* ATCC29213, respectively) by broth dilution method. The bacterial strains were maintained and nutrient agar media (NA). In preparation for the study, a homogeneous suspension of NPs was prepared by sonication for 15–20 min at 30 °C, ranging in the concentration from 250 to 15.62 $\mu\text{g mL}^{-1}$. Mueller-Hinton (MHB) was used to grow test organisms for overnight at 37 °C and subsequently adjusted to the cell frequency of 10^6 CFU mL^{-1} . The adjusted inoculum of each bacterial strain was added to the solution of MHB with NPs and incubated with

shaking at 37 °C for 24 h. Untreated bacteria was used as a negative control. The MIC was recorded as the least concentration of NPs, which had no growth visible in the broth (absence of turbidity).

Following the MIC evaluation, MBC was obtained by taking an aliquot of the MIC for further plating on the MHA plates. The inoculated plates were further incubated for overnight at 37 °C and the MBC was taken as the concentration at which no growth or CFU less than 3 was obtained.¹⁹

2.7. Study of topological changes in treated bacteria

Additionally, the treated culture of *E. coli* and *S. aureus* were studied by SEM for the morphological and physiological alteration caused by NPs. Precisely, adjusted bacterial cells were treated at the concentration obtained as its MIC and subjected to incubation at 37 °C for overnight. Untreated samples were included as the negative control. Later treated and untreated cells were centrifuged at 12 000 rpm for 10 min. The harvested cells were thrice washed using PBS and primarily fixed using 2.5% glutaraldehyde for 4 h, then again fixed with 1% osmium tetroxide for 1–2 h. Cells were washed multiple times and further dehydrated by varying conc. of ethanol (50%, 70%, 90%, 100%). The cells were placed on aluminum stubs and dried using desiccator. Finally, gold coating was done and cells were examined by SEM at an accelerating voltage of 20 kV.¹⁹

2.8. Antiproliferative activity

2.8.1. Cell culture & treatments. Human colorectal carcinoma cells (HCT-116) were used for the study. DMEM medium was used which was supplemented with 10% fetal bovine serum (FBS); (10%) L-glutamine; 10% selenium chloride; 120 $\mu\text{g mL}^{-1}$ and streptomycin; and 120 units per mL penicillin in 5% CO_2 incubator (Thermo Scientific Heracell-150) at temperature 37 °C. The cells with more than 70–80% confluence was used for the TiO_2 and AgNPs treatments. The treatment of HCT-116 cells were carried out with different concentrations of 0.5 to 8.0 $\mu\text{g mL}^{-1}$. The cells were observed after the time span of 48 h. Experiment was carried out in triplicate for statistical analysis.²⁰

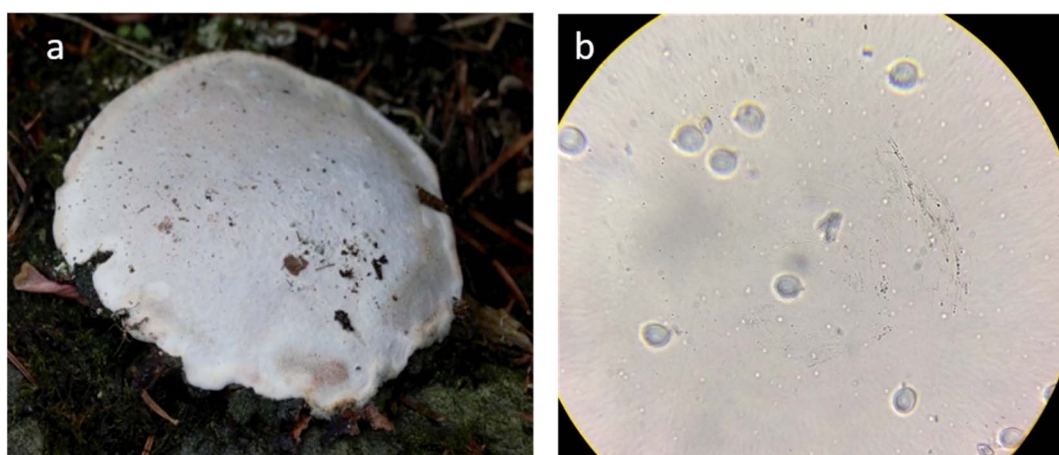


Fig. 1 Photographs of brown rot basidiomycetes: *F. pinicola*, (a) under view showing pores (b) basidiospores at 40 \times .



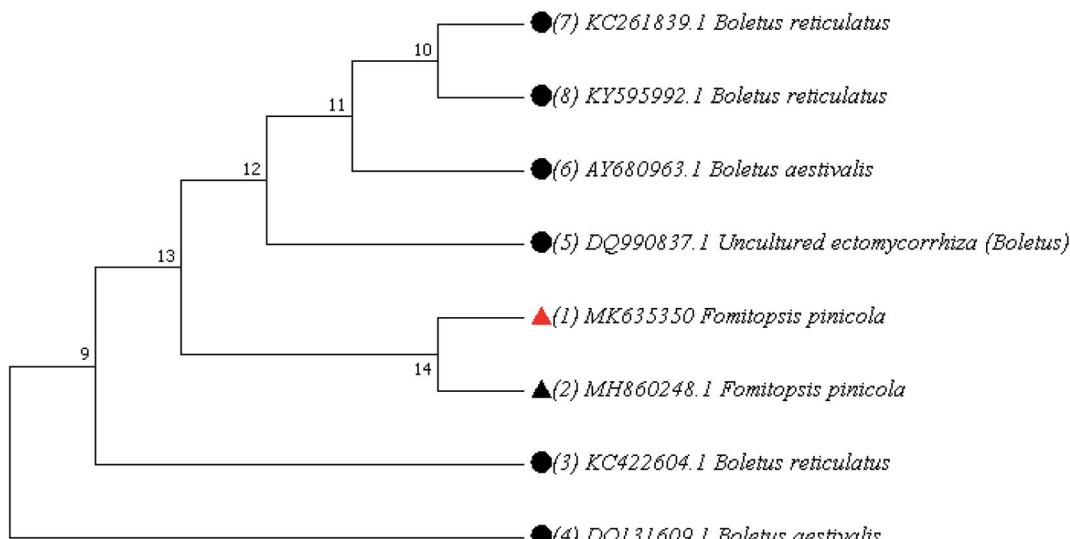


Fig. 2 Phylogenetic tree of *F. pinicola* indicated as ▲.

2.8.2. Cancer cell morphology. The cell morphology of untreated and treated HCT-116 cells were examined post 48 h under inverted microscope (TS100F-Eclipse, Nikon) and compared under 200 \times magnifications.

2.8.3. Cytotoxicity by MTT assay. The cells with confluence of 70–80% in 96-well cell culture plates were subjected to MTT assay. After 48 h, MTT (5 mg mL⁻¹) was added in all the wells and kept for 4 h. Later, DMSO was added and plate was read in ELISA Plate Reader 570 nm wavelength (Biotek Instruments, USA).²⁰ The (%) percentage of cell viability was calculated as per given formula:

$$\% \text{ cell viability} = \frac{\text{optical density of nanoparticles}}{\text{optical density of controls}} \times 100$$

2.8.4. Nuclear staining by DAPI. The cells were stained with DAPI staining to study the effect of TiO₂ NPs and Ag NPs on the cell nucleus. After 48 h, the treated and untreated HCT-116 cells were immersed in an ice-cold (4%) paraformaldehyde. Later, the cells were added with Triton X-100 prepared in PBS for 5 min to premetallize the cell membrane. The cells were stained

using DAPI (5 μ g mL⁻¹) in PBS, prepared in dark. Washing with Triton X-100 was done, followed by examining the nuclear morphology under confocal scanning microscope (Zeiss, Germany) equipped with digital camera.²⁰

In the present study, cell viability data were presented as mean (\pm) standard deviation (SD) which were obtained from three independent experimental repeats. One-way ANOVA followed by Dunnett's *post hoc* test with GraphPad Prism software (GraphPad Software, Inc., La Jolla, CA, USA) for the statistical analysis. $P < 0.05$ was considered to indicate a statistically significant difference.

3. Results

3.1. Phenotypic and genotypic studies of *F. pinicola*

The phenotypic analysis of mushroom namely *F. pinicola* was done. Spores are 5.5–7 \times 4.0–5.0 μ m, oval, smooth: spore print pale yellow. Spores are bilaterally symmetrical. The shape of the hilar appendix is beaked (Fig. 1a and b). This was further confirmed by phylogenetic analysis of the ITS1–ITS4 sequences of the mushroom, which was deposited in the NCBI Gene Bank

Table 1 Gene bank accession numbers and top BLAST match sequences of the mushroom isolates along with maximum identity, query coverage

Accession number	BLAST match sequence		
	Reference accession number	Coverage	Maximum identity
MK635350	MH860248.1 <i>Fomitopsis pinicola</i>	100%	100%
	KC422604.1 <i>Boletus reticulatus</i>	99%	98.75%
	DQ131609.1 <i>Boletus aestivalis</i>	99%	98.75%
	DQ990837.1 Uncultured mycorrhiza	98%	98.99%
	KY595992.1 <i>Boletus reticulatus</i>	91%	99.18%
	AY680963.1 <i>Boletus aestivalis</i>	89%	98.88%
	KC261839.1 <i>Boletus reticulatus</i>	71%	99.47%



under accession number MK635350. The phylogenetic relationships with related species have been shown in Fig. 2, presenting the similarity score of 100% to *F. pinicola* (MH860248.1) (Table 1).

3.2. Characterization of biosynthesized TiO_2 and Ag NPs

The production of TiO_2 and Ag NPs mediated by *F. pinicola* was indicated by examining the color change in the reaction mixture. Fig. 3 shows the XRD spectra of (a) TiO_2 and (b) Ag NPs. The formation of crystalline TiO_2 with sharp peaks corresponding to rutile phase was observed using the extract of *F. fomentarius*. In case of TiO_2 synthesis using *F. pinicola* (Fig. 3a), a reduced crystallinity and broadness of peaks indicates nano-sized TiO_2 formation with major phase of rutile. Fig. 3b shows the XRD spectra of Ag NPs. The spectra showed a clear diffraction lines corresponding to (111), (200) and (220) planes indicating the presence of Ag NPs.²¹ The presence of unidentified peak at about 57.5° could be attributed to the crystalline components present in the extract.

The presence of active ingredients like polyphenols and flavonoids in the mushroom extract play a key role as bio reductant in reducing metal ions of metal source to nanoparticles. Fig. 4 shows the FT-IR spectroscopy of (a) TiO_2 and (b) Ag NPs. In case of TiO_2 , the hydroxyl functional group absorption coordinated TiO_2 species was observed with distinct peaks at 1664 cm^{-1} and 3480 cm^{-1} . The presence of TiO_2 was further confirmed with absorption peak of Ti–O bands at about 460, 597 and 777 cm^{-1} . In case of Ag NPs, presence of difference functional groups corresponding to N–H, O–H, and methylene C–H was observed between $1000\text{--}3700\text{ cm}^{-1}$ (Fig. 4b). A distinct broad peak appears between $3650\text{--}2400\text{ cm}^{-1}$ corresponding to hydroxyl (–OH), N–H stretching of primary amines and methylene (CH_2). The presence of asymmetrical C–O stretching peak was observed 1632 cm^{-1} . The presence of aromatic ring (–C–C–) and aliphatic amine (C–N) was clearly seen with an intense absorption peak at about 523 cm^{-1} and 1040 cm^{-1} . In both cases, the presence of elongated peaks at fingerprint region between $1000\text{--}1800\text{ cm}^{-1}$ showed several functional group moieties of mushroom extract. The linear aliphatic amines (C–N) showed peak absorption at $1000\text{--}1040\text{ cm}^{-1}$. The functional

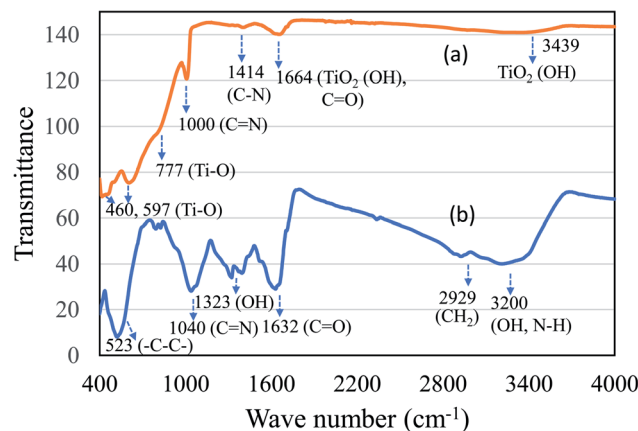


Fig. 4 FT-IR spectra of (a) TiO_2 and (b) Ag NPs.

group analysis study using FT-IR indicates that active components (amino, hydroxyl and methyl) in mushroom act as an effective bio reductant to produce TiO_2 and Ag NPs.

The coordination sites of TiO_2 and Ag NPs prepared using *F. pinicola* was studied using diffuse reflectance UV-visible spectroscopy. In case of TiO_2 NPs, isolated tetrahedral Ti^{4+} species was observed with a band at about 220 nm (Fig. 5a). The presence of distinct peaks corresponding to rutile and octahedral Ti compounds were observed between $250\text{--}420\text{ nm}$. The presence of anatase (titania) phase was also reported at about 350 nm . The result coincides with XRD analysis, which indicated the presence of rutile and anatase phase of TiO_2 . The presence of few agglomerated TiO_2 species were also observed between $500\text{--}600\text{ nm}$. In case of Ag NPs, the sample exhibited presence of three kinds of Ag species indicating the variation in coordination environments (Fig. 5b). A weak absorption at about 224 nm indicates presence of few Ag^+ species. However, the strong absorption at 352 nm showed presence of $\text{Ag}_n^{\delta+}$ nanoclusters as predominant species followed by Ag^0 with absorption maxima ranging between $410\text{--}540\text{ nm}$.

Fig. 6 demonstrated SEM and TEM morphology of TiO_2 and Ag NPs. For TiO_2 NPs, surface features and distribution have been examined through SEM (Fig. 6a). SEM micrographs showed that these nanoparticles are dispersed in irregular distribution with rough surface. TEM (Fig. 6b) showed irregular

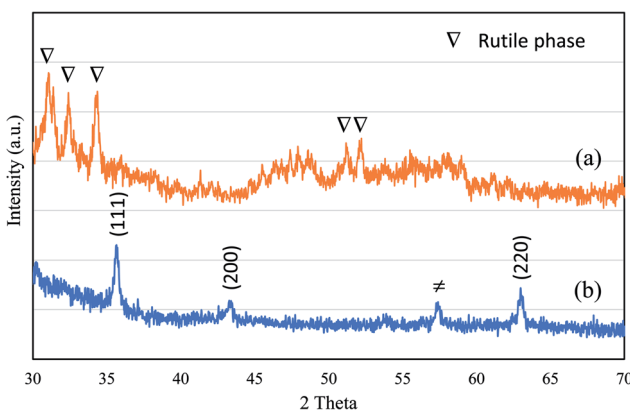


Fig. 3 X-ray diffraction spectra of (a) TiO_2 and (b) Ag NPs.

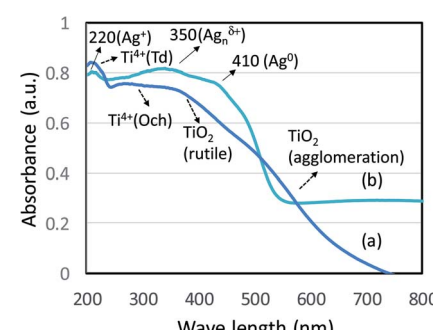


Fig. 5 (a and b) shows the diffuse reflectance spectra of TiO_2 and Ag NPs.



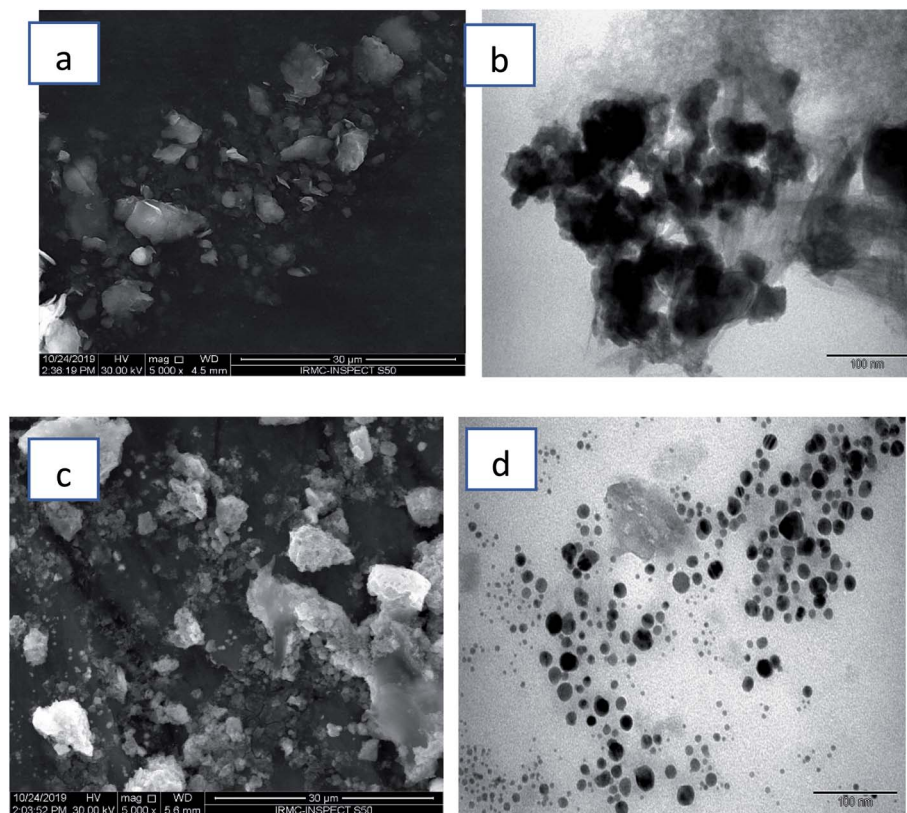


Fig. 6 (a) SEM and (b) TEM images of TiO₂ NPs; (c) SEM and (d) TEM images of Ag NPs.

shape and size. On the other hand, Fig. 6c illustrated spherical Ag nanoparticles with some agglomeration of nanoparticles, while TEM (Fig. 6d) depicted well distribution of small spherical nanoparticles with average diameter ranging from 10–30 nm.

3.3. Antibacterial activity of synthesized NPs

The assay was performed by examining the MIC and MBC values, against *E. coli* and *S. aureus*. On treatment with TiO₂ NPs,

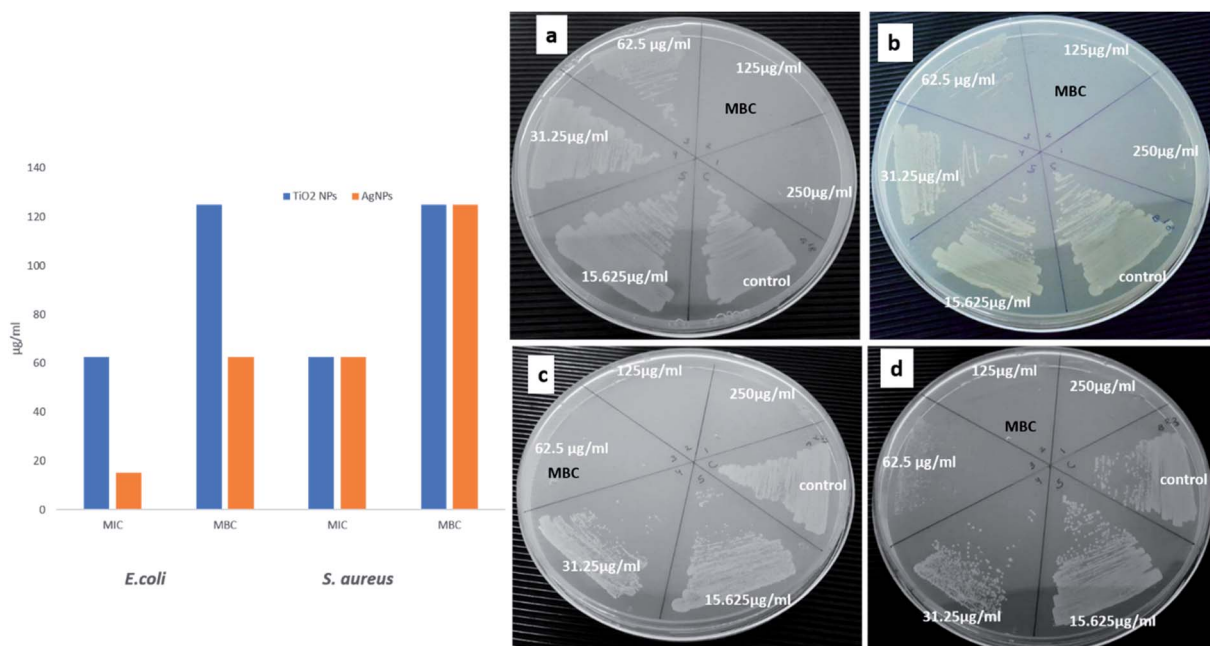


Fig. 7 MIC/MBC assay: (a) *E. coli* and (b) *S. aureus* treated with different conc. of TiO₂ NPs; (c) *E. coli* and (d) *S. aureus* treated with different conc. of Ag NPs.



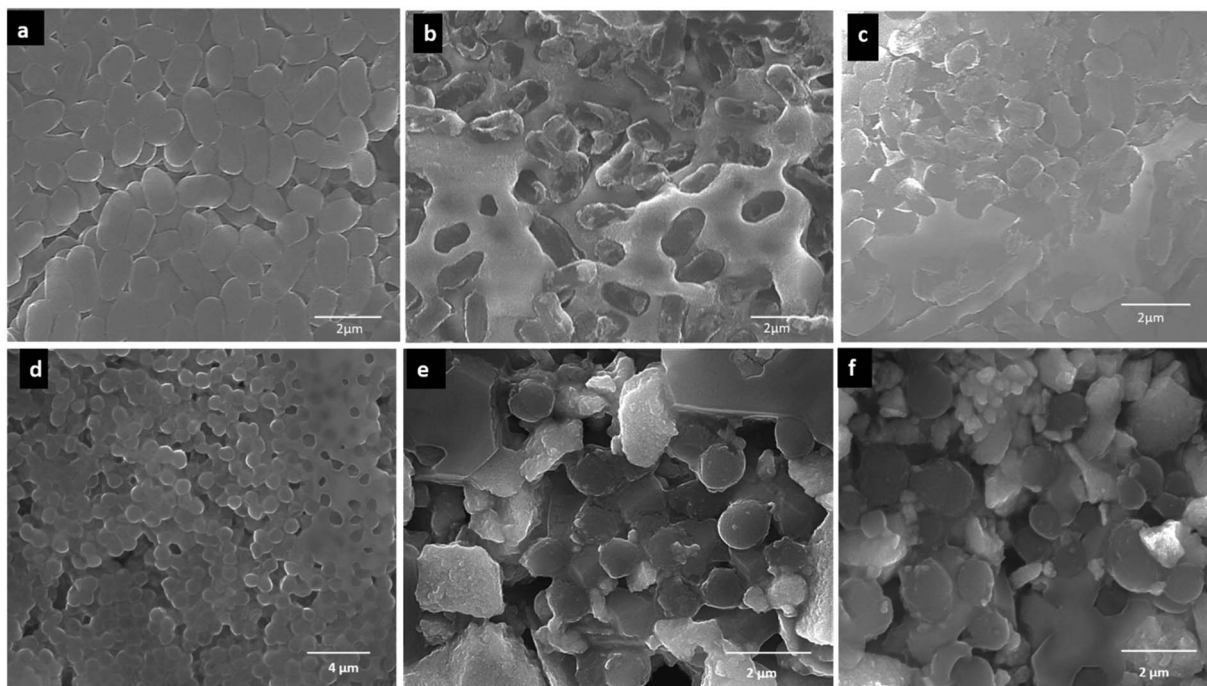


Fig. 8 SEM micrographs of treated bacteria at concentration obtained as its MIC (a) *E. coli* control (untreated cells); (b) *E. coli* treated TiO_2 NPs; (c) *E. coli* treated Ag NPs; (d) *S. aureus* control (untreated cells); (e) *S. aureus* treated TiO_2 NPs; (f) *S. aureus* treated Ag NPs.

the MIC/MBC values were $62.5/125$ and $62.5/125 \mu\text{g mL}^{-1}$ for *E. coli* and *S. aureus*, respectively (Fig. 7a and b). Whereas, Ag NPs, the MIC/MBC values obtained were $15.62/62.5$ and $62.5/125 \mu\text{g mL}^{-1}$ for *E. coli* and *S. aureus*, respectively (Fig. 7c and d). Both the biosynthesized NPs were found to have a significant activity

against both the organism, although improved activity was obtained with Ag NPs against *E. coli*.

3.4. Study of topological changes in treated bacteria

Morphological changes induced by synthesized TiO_2 and Ag NPs to the test bacteria were further studied by SEM. The

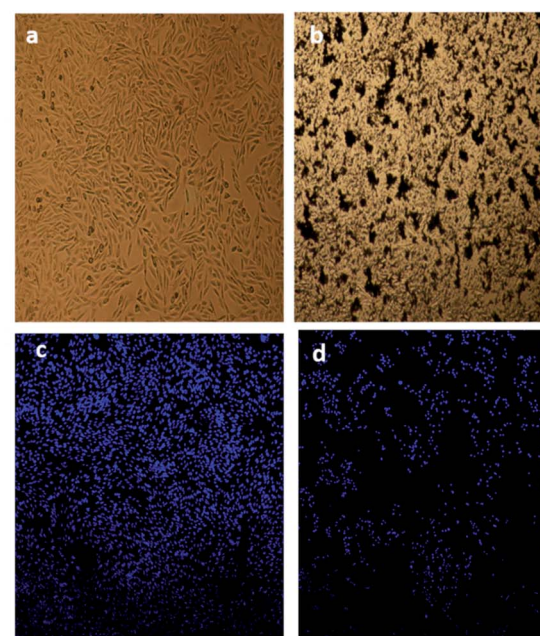
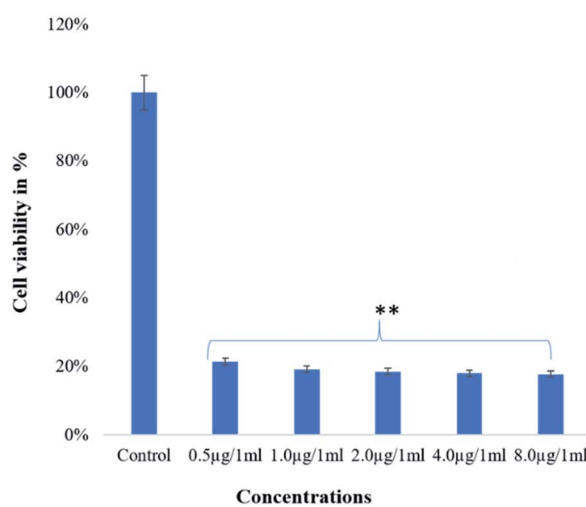


Fig. 9 Cell viability of HCT-116 cells by MTT assay on treatment with TiO_2 NPs after 48 h and cell morphology analysis (a) control; (b) treated with $8.0 \mu\text{g mL}^{-1}$, analyzed by light microscope. (c) Control, & (d) treated $8.0 \mu\text{g mL}^{-1}$ analyzed by confocal scanning microscope. Data are the mean \pm SD of three different experiments. Difference between two treatment groups were analysed by Student's *t* test where $^{**}p < 0.01$, *p*-values were calculated by Student's *t*-test. No changes were observed in control group.



control (untreated) *E. coli* cells, appeared as normal rod-shaped with a consistent and smooth cell surface (Fig. 8a). Although, treated *E. coli* with both the NPs was not found intact, with irregularities at cell surfaces seen. The Ag NPs treated cells were seen more damaged than that of the TiO_2 NPs treated cells. The treatment of *E. coli* cells with TiO_2 NPs produced a mild alteration (Fig. 8b), whereas Ag NPs treated *E. coli* was severely affected (Fig. 8c). Simultaneously, the untreated *S. aureus* cells (control) were normal in shape *i.e.*, cocci with smooth cell surface (Fig. 8d). The treated *S. aureus* cells on the contrary were seen with irregularities and distorted cell surface. Both the TiO_2 and Ag NPs had nearly similar outcome on the Gram-positive bacteria (Fig. 8e and f).

3.5. Antiproliferative activity

The dose-depended effects on cancer cells survivability was found as examined by MTT assay. The treatment of TiO_2 NPs showed strong cytotoxic effects on cancer cell viability as more majority of the cells were found dead after treatments of lower $0.5 \mu\text{g mL}^{-1}$ (Fig. 9). TiO_2 NP treated cells showed significant alteration in structure and the cell nucleus as revealed by light and confocal microscopy (Fig. 9b and d). It was clearly indicated that nucleus has disintegrated, and also nuclear condensation was observed, along with the death of many cancer cells. It was observed that TiO_2 NPs-treatment caused significant loss of nuclear staining in the HCT-116 cells as seen by DAPI staining (Fig. 9a and c).

The treatment of AgNPs also showed strong cytotoxic effects on cancer cells viability as more majority of the cells were found dead after the treatment of $0.5 \mu\text{g mL}^{-1}$ (Fig. 10). AgNPs exhibited significant deformities in cell morphology and the

nucleus as revealed by light and confocal microscopy (Fig. 10b and d). The clear evidence of disintegration and condensation of nucleus was observed and as many cells were found dead. The Ag NPs-treatment caused significant loss of nuclear staining in the HCT-116 cells as seen by DAPI staining (Fig. 10d) with compared to control cells (Fig. 10a and c).

4. Discussion

The phenotypic analysis of mushroom collected from the Kashmir Himalayas indicated to be a brown-rot fungus namely *F. pinicola*, which fills Basidiomycota, Agaricomycetes, Fomitopsidaceae. This common fungal species is a wood colonizing saprotroph found in boreal and temperate forests of the Northern Hemisphere (Fig. 1a). It has a heterothallic sexual system having two haploid mycelia which produce a dikaryotic mycelium to complete the sexual cycle.²²

Edible mushrooms are known to harbor various bioactive compounds with enormous activities like antioxidant, anti-inflammatory, antimicrobial, hepato protective, hypotensive and anticancer activities.²³ Based on these properties, an attempt was made to synthesize TiO_2 and Ag NPs by using the cell free extract of *F. pinicola* as a reducing agent. The production of TiO_2 and Ag NPs was indicated by examining the color change in the reaction mixture which was confirmed by the XRD spectra. The peak intensity of both TiO_2 , and Ag NPs was studied and observed as per the previous studies by Rajakumar *et al.* and Sriramulu and Sumathi, respectively.^{21,24} The FT-IR spectra showed several functional groups presence in mushroom species assisting TiO_2 and Ag NPs formation.^{25,26} The study showed the presence of various components related to

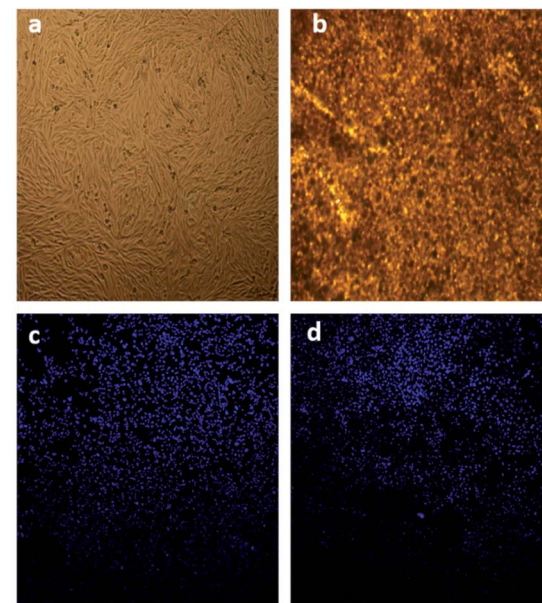
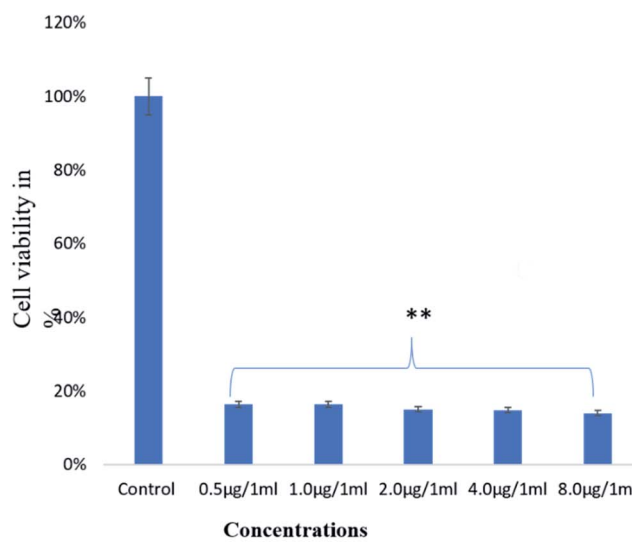


Fig. 10 Cell viability of HCT-116 cells by MTT assay on treatment with Ag NPs after 48 h and cell morphology analysis (a) control; & (b) treated with $8.0 \mu\text{g mL}^{-1}$, analyzed by light microscope. (c) Control, & (d) treated $8.0 \mu\text{g mL}^{-1}$ analyzed by confocal scanning microscope. Data are the mean \pm SD of three different experiments. Difference between two treatment groups were analysed by Student's *t* test where $**p < 0.01$, *p*-values were calculated by Student's *t*-test. No changes were observed in control group.



amino, methyl and hydroxyl group present in mushroom that assist in transformation of titanium oxide and silver nanoparticles. The samples using DRS-UV showed presence of isolated Ti^{4+} species corresponding to tetrahedral coordination²⁷ and Ag NPs, exhibited presence of three kinds of Ag species indicating the variation in coordination environments.²⁸ SEM and TEM morphology of TiO_2 and Ag NPs showed irregular shape and size²⁹ and agglomeration of nanoparticles with distribution of small spherical nanoparticles (10–30 nm),³⁰ respectively.

Broth dilution method was used to evaluate the toxicity of a synthesized TiO_2 and Ag NPs to bacterial cells and hence the susceptibility of the cells in this mixture. The antimicrobial action of Ag NPs has been well studied and successfully used in the pharmaceutical industries for healing of wounds and as antibiotic applications.³¹ TiO_2 NPs has also been reported for significant reduction in the number of *Pseudomonas* colonies.³² The current study is also supported by the studies carried out by Swathi *et al.* presenting the green synthesized TiO_2 NPs, against Gram-negative and positive organisms, resulting in enhanced activity against Gram negative bacteria.³³

This study was aimed to find the antibacterial potential of biologically synthesized TiO_2 and Ag NPs against *E. coli* and *S. aureus*. Both the biosynthesized NPs were found to have a significant activity against both the organism, although improved activity was obtained with Ag NPs against *E. coli*. The obtained results are in agreement with the number of studies conducted previously stating the antibacterial activity of bio-synthesized Ag NPs.^{7–11,31}

Morphological changes induced by synthesized TiO_2 and Ag NPs to the test bacteria indicated that the Gram negative *E. coli* cells were more adversely affected as that of the Gram positive *S. aureus*. The achieved results demonstrated that the greater activity of Ag NPs, synthesized by green approach could be due to their spherical shape and smaller size of 10–30 nm, as compared to TiO_2 NPs having a larger size of 80–120 nm. The elevated activity might also be facilitated by the efficient attachment of Ag NPs, to the bacterial cell surface, and hence play a crucial role in obtaining significant antibacterial activity. However, many studies have been carried out for the antimicrobial action of Ag NPs, still the exact mechanism of action is not clear.^{34,35} Various studies hypothesized the interaction of electrostatic forces between the negatively charged bacterial cell surface and the positively charged NPs.^{36–38} Additionally, the antimicrobial efficiency of NPs can be also owed to many hindered potential metabolic reactions, like inactivated proteins and enzymes, DNA degradation and so on.^{11,39} Ag NPs have been recorded to interact with the proteins having phosphorous and sulfur moieties as the cell component and genetic materials.^{40–42} Therefore, the successful application of these NPs depends on the controlled size and shape, which offers the enhanced surface area, having a huge impact on various cellular and metabolic processes.³⁶

The impact of TiO_2 and Ag NPs was studied both morphologically using light and confocal microscope and quantitatively by MTT assay. The dose-dependent effects on cancer cells survivability was found as examined by MTT assay. The clear

evidence of disintegration and condensation of nucleus was observed and as many cells were found dead. The Ag NPs-treatment caused significant loss of nuclear staining in the HCT-116 cells as seen by DAPI staining. The treatment of nanoparticles also showed strong cytotoxic effects on cancer cells viability as more majority of the cells were found dead after treatments of nanoparticles. The mechanism through which cancer cells die could be attributed to program cell death, as we have seen that cancer cells were undergone nuclear disintegration, and DNA fragmentation after nanoparticles treatment. This programmed cell death or apoptosis is major marker for the cancer cell death. However, it is of paramount importance to study the molecular pathways involved in NPs mediated cancer cell death. Interestingly, there are several reports of NPs, which are known to induce fragmentation and disintegration of nucleus in cancer cells.^{43–45}

5. Conclusion

Therefore, present study of green synthesis of NPs offers convincing antibacterial activity against the Gram-negative and Gram-positive bacteria, which could be a boon for treating the infectious diseases and can be utilized in food industry to minimize the contamination and extend the duration for preservation. Additionally, the cytotoxic activity holds the potential as a promoter for human colon cancer therapy.

Author contributions

S. Rehman, conceptualized and designed the study, Suriya Rehman, Romana Farooq, Sarah Mousa Asiri, Firdos Alam Khan, Rabindran Jermy, M. A. Ansari and Zainab Alsalem carried out the experiments and prepared all figures. Suriya Rehman, Vijaya Ravinayagam, M. A. Shah and Reem Al Jindan discussed the results and wrote the first draft. Firdos Alam Khan, Suriya Rehman and Rabindran Jermy revised and edited the manuscript. All the authors have read and approved the final manuscript.

Finance support

Financial support is acknowledged from Deanship of Scientific Research, Imam Abdulrahman Bin Faisal University, Dammam, Saudi Arabia, under Project No. 2019-072-IRMC.

Availability of data and material

The data analyzed are available from the corresponding author upon a request.

Conflicts of interest

No potential conflict of interest is reported by authors.



References

1 M. Haase and H. Schäfer, Upconverting nanoparticles, *Angew. Chem., Int. Ed.*, 2011, **50**(26), 5808–5829.

2 D. L. Fedlheim and C. A. Foss, *Metal nanoparticles: synthesis, characterization, and applications*, CRC Press, 2001.

3 L. Liu and A. Corma, Metal catalysts for heterogeneous catalysis: from single atoms to nanoclusters and nanoparticles, *Chem. Rev.*, 2018, **118**(10), 4981–5079.

4 R. Dobrucka, Synthesis of titanium dioxide nanoparticles using *Echinacea purpurea* herba, *Iran. J. Pharm. Res.*, 2017, **16**(2), 756.

5 D. Chandra, T. General and S. Chandra, Microorganisms: an asset for decontamination of soil, in *Smart Bioremediation Technologies*, Elsevier, 2019, pp. 319–345.

6 K. Jhansi, *et al.*, Biosynthesis of MgO nanoparticles using mushroom extract: effect on peanut (*Arachis hypogaea* L.) seed germination, *3 Biotech*, 2017, **7**(4), 263.

7 A. A. Kareem and A. H. Al-Hamadani, Combination effect of edible mushroom-sliver nanoparticles and antibiotics against selected multidrug biofilm pathogens, *Iraq Medical Journal*, 2017, **1**(3), 68–74.

8 G. Narasimha, *et al.*, Mushrooms (*Agaricus bisporus*) mediated biosynthesis of sliver nanoparticles, characterization and their antimicrobial activity, *Int. J. Nano Dimens.*, 2011, **2**(1), 29.

9 G. V. Anehosur, *et al.*, Synthesis and determination of antimicrobial activity of visible light activated TiO₂ nanoparticles with polymethyl methacrylate denture base resin against *Staphylococcus aureus*, *J. Gerontol. Geriatr. Res.*, 2012, **1**(1), 1–8.

10 K. J. P. Anthony, *et al.*, Synthesis of silver nanoparticles using pine mushroom extract: a potential antimicrobial agent against *E. coli* and *B. subtilis*, *J. Ind. Eng. Chem.*, 2014, **20**(4), 2325–2331.

11 Y. Mohanta, *et al.*, Silver nanoparticles synthesized using wild mushroom show potential antimicrobial activities against food borne pathogens, *Molecules*, 2018, **23**(3), 655.

12 M. Eskandari-Nojedehi, H. Jafarizadeh-Malmiri and J. Rahbar-Shahrouzi, Hydrothermal green synthesis of gold nanoparticles using mushroom (*Agaricus bisporus*) extract: physico-chemical characteristics and antifungal activity studies, *Green Process. Synth.*, 2018, **7**(1), 38–47.

13 N. Park and S.-S. Park, Purification and characterization of a novel laccase from *Fomitopsis pinicola* mycelia, *Int. J. Biol. Macromol.*, 2014, **70**, 583–589.

14 D. Krueger, *Monographic studies in the genus Polyporus (Basidiomycotina)*, 2002.

15 S. Rehman, *et al.*, Comparative studies and identification of camptothecin produced by an endophyte at shake flask and bioreactor, *Nat. Prod. Res.*, 2009, **23**(11), 1050–1057.

16 P. Dresch, *et al.*, Fungal strain matters: colony growth and bioactivity of the European medicinal polypores *Fomes fomentarius*, *Fomitopsis pinicola* and *Piptoporus betulinus*, *AMB Express*, 2015, **5**(1), 4.

17 J. Felsenstein, *PHYLIP (phylogeny inference package), version 3.5 c*, 1993.

18 S. Rehman, *et al.*, Isolation and characterization of a novel thermophile; *Bacillus haynesii*, applied for the green synthesis of ZnO nanoparticles, *Artif. Cells, Nanomed., Biotechnol.*, 2019, **47**(1), 2072–2082.

19 S. Akhtar, *et al.*, Synthesis of Mn_{0.5}Zn_{0.5}Sm_xEu_xFe_{1.8-2x}O₄ Nanoparticles *via* the Hydrothermal Approach Induced Anti-Cancer and Anti-Bacterial Activities, *Nanomaterials*, 2019, **9**(11), 1635.

20 F. Khan, *et al.*, FMSP-nanoparticles induced cell death on human breast adenocarcinoma cell line (MCF-7 cells): morphometric analysis, *Biomolecules*, 2018, **8**(2), 32.

21 M. Sriramulu and S. Sumathi, Photocatalytic, antioxidant, antibacterial and anti-inflammatory activity of silver nanoparticles synthesised using forest and edible mushroom, *Adv. Nat. Sci.: Nanosci. Nanotechnol.*, 2017, **8**(4), 045012.

22 A. V. Shnyreva, S. M. Badalyan and A. A. Shnyreva, Analysis of Intraspecies Genetic Variability among Collections of Medicinal Red Belt Conk Mushroom, *Fomitopsis pinicola* (Agaricomycetes), *Int. J. Med. Mushrooms*, 2019, **21**(3), 291–300.

23 S. Watanabe and M. Uehara, Health Effects and Safety of Soy and Isoflavones, in *The Role of Functional Food Security in Global Health*, Elsevier, 2019, pp. 379–394.

24 G. Rajakumar, *et al.*, Fungus-mediated biosynthesis and characterization of TiO₂ nanoparticles and their activity against pathogenic bacteria, *Spectrochim. Acta, Part A*, 2012, **91**, 23–29.

25 X. Wang, *et al.*, The study of titanium dioxide modification by glutaraldehyde and its application of immobilized penicillin acylase, *Colloids Surf., A*, 2019, **560**, 298–305.

26 M. Govarthanan, *et al.*, Biosynthesis and characterization of silver nanoparticles using panchakavya, an Indian traditional farming formulating agent, *Int. J. Nanomed.*, 2014, **9**, 1593.

27 B. C. Ledesma, *et al.*, Hydrogenation of Tetralin Over Ir Catalysts Supported on Titania-Modified SBA-16, *Catal. Lett.*, 2014, **144**(5), 783–795.

28 I. A. Khan, *et al.*, CO Oxidation Catalyzed by Ag Nanoparticles Supported on SnO/CeO₂, *J. Braz. Chem. Soc.*, 2015, **26**, 695–704.

29 E. Demir, A. Creus and R. Marcos, Titanium dioxide and zinc oxide nanoparticles are not mutagenic in the mouse lymphoma assay but modulate the mutagenic effect of UV-C-light post-treatment, *Fresenius Environ. Bull.*, 2017, **26**, 1001–1016.

30 R. Kotcherlakota, S. Das and C. R. Patra, Therapeutic applications of green-synthesized silver nanoparticles, in *Green Synthesis, Characterization and Applications of Nanoparticles*, Elsevier, 2019, pp. 389–428.

31 U. K. Parashar, P. S. Saxena and A. Srivastava, Bioinspired synthesis of silver nanoparticles, *Dig. J. Nanomater. Bios.*, 2009, **4**(1), 1.



32 G. Lusvardi, *et al.*, Synthesis and characterization of TiO_2 nanoparticles for the reduction of water pollutants, *Materials*, 2017, **10**(10), 1208.

33 N. Swathi, D. Sandhiya, S. Rajeshkumar and T. Lakshmi, *Int. J. Res. Pharm. Sci.*, 2019, **10**, 856–860.

34 R. Al-Bahrani, *et al.*, Green synthesis of silver nanoparticles using tree oyster mushroom *Pleurotus ostreatus* and its inhibitory activity against pathogenic bacteria, *Mater. Lett.*, 2017, **186**, 21–25.

35 A. Ashour, *et al.*, Antimicrobial activity of metal-substituted cobalt ferrite nanoparticles synthesized by sol-gel technique, *Particuology*, 2018, **1**(40), 141–151.

36 K. Anandan and V. Rajendran, Size controlled synthesis of SnO_2 nanoparticles: facile solvothermal process, *Journal of Non-oxide Glasses*, 2010, **2**, 83–89.

37 P. Balashanmugam, *et al.*, Mycosynthesis, characterization and antibacterial activity of silver nanoparticles from *Microporusxanthopus*: a macro mushroom, *Int. J. Innov. Res. Sci. Eng. Technol.*, 2013, **2**(11), 6262–6270.

38 C. Wang, *et al.*, Green synthesis of silver nanoparticles by *Bacillus methylotrophicus*, and their antimicrobial activity, *Artif. Cells, Nanomed., Biotechnol.*, 2016, **44**(4), 1127–1132.

39 S. Birla, *et al.*, Fabrication of silver nanoparticles by *Phoma glomerata* and its combined effect against *Escherichia coli*, *Pseudomonas aeruginosa* and *Staphylococcus aureus*, *Lett. Appl. Microbiol.*, 2009, **48**(2), 173–179.

40 S. Prabhu and E. K. Poulose, Silver nanoparticles: mechanism of antimicrobial action, synthesis, medical applications, and toxicity effects, *Int. Nano Lett.*, 2012, **2**(1), 32.

41 A. Ivask, *et al.*, Size-Dependent Toxicity of Silver Nanoparticles to Bacteria, Yeast, Algae, Crustaceans and Mammalian Cells *In Vitro*, *PLoS One*, 2014, **9**(7), e102108.

42 M. Griffith, *et al.*, *Silver Nanoparticle Applications: In the Fabrication and Design of Medical and Biosensing Devices*, 2015.

43 K. Murugesan, *et al.*, Effects of green synthesised silver nanoparticles (ST06-AgNPs) using curcumin derivative (ST06) on human cervical cancer cells (HeLa) *in vitro* and EAC tumor bearing mice models, *Int. J. Nanomed.*, 2019, **14**, 5257.

44 S. Rehman, *et al.*, Synthesis and biological characterization of $Mn_{0.5}Zn_{0.5}Eu_xDy_xFe_{1.8-2x}O_4$ nanoparticles by sonochemical approach, *Mater. Sci. Eng., C*, 2019, 110534.

45 F. A. Khan, *et al.*, Targeted delivery of poly(methyl methacrylate) particles in colon cancer cells selectively attenuates cancer cell proliferation, *Artif. Cells, Nanomed., Biotechnol.*, 2019, **47**(1), 1533–1542.

